ACI STRUCTURAL JOURNAL TECHNICAL PAPER

Title No. 121-S24

Outrigger Action in Tall Core-Wall Buildings with Flat-Plate Framing

by Connie I. Chen and Jack P. Moehle

In tall core-wall buildings with concrete unbonded post-tensioned flat-plate gravity framing, modeling the behavior of the slab-wall-column framing under earthquake loading can be crucial to determining structural response quantities for the design of the flat-plate framing. The outrigger action of the gravity system also affects the overall dynamic properties of the building and may affect wall moment and shear demands. The outrigger effect can be modeled using a slab-beam model, which uses linear-elastic frame elements with concentrated nonlinear hinges at each end. In this study, the slab-beam model is calibrated using results from a slab-wall-column laboratory test. Recommendations suitable for design-office practice are presented.

Keywords: earthquake engineering; flat plate; gravity framing; nonlinear modeling; outrigger action; plastic hinge; post-tensioned slab; slab-column joint; slab-wall connection.

INTRODUCTION

Reinforced concrete core walls are a prevalent seismic-force-resisting system in tall buildings. The typical layout is a centrally located core wall surrounded by gravity framing, which often consists of concrete unbonded post-tensioned slab-column framing. The slab-column framing acts as an outrigger for the overall building and thereby contributes to the overall overturning resistance. The resulting accumulation of axial forces on the perimeter columns can potentially be large enough to control the column design. For these reasons, guidelines for tall building design (PEER TBI 2017; LATBSDC 2020) recommend that gravity framing be included in the dynamic analysis model to obtain the best estimate of the expected response.

ASCE/SEI 7-16 (2017) and ACI 318-19 (ACI Committee 318 2019) require gravity systems to be designed for gravity loads, including vertical seismic load effects. ASCE/SEI 7 also requires the gravity system under risk-targeted maximum considered earthquake (MCE_R) loading to satisfy deformation compatibility using the mean building displacements from the suite of nonlinear response-history analyses. The current prescriptive provisions of the building code are based on a traditional approach that requires that the prescribed lateral forces be resisted by vertical elements of the seismic-force-resisting system that have been detailed to be capable of lateral force resistance without critical strength decay. For reinforced concrete, only special moment frames and special structural walls (and not flat-plate frames) are permitted to resist prescribed lateral earthquake forces.

The coupling between a core wall and slab-column framing can be modeled by including equivalent slab-beams connecting the core walls to the perimeter columns. The slab-beam model can be an assembly of a linear-elastic frame element, representing the effective stiffness of the slab, and nonlinear moment-rotation hinges at both ends, representing the post-yield response of the slab-wall and slab-column connections. In this study, the stiffness and strength of the slab-beams are calibrated using test results reported by Klemencic et al. (2006). An example calculation using a typical story of a tall core-wall building with flat-plate gravity framing shows the importance of considering the "outrigger effect" when determining column axial forces for design.

RESEARCH SIGNIFICANCE

This study proposes a model for the stiffness and strength of slab-wall-column outrigger framing systems calibrated by laboratory test data. An example calculation of the outrigger effect on column axial force in a typical story of a tall core-wall building shows the potential importance of including the slab outrigger effect in design.

STRUCTURAL SYSTEM DESCRIPTION

This study is developed considering a 40-story-tall archetypal building with the floor plan shown in Fig. 1. The structural system includes a centrally located core wall, which supports gravity loads and is the primary lateral-force-resisting system, and slab-column framing, which is intended primarily to support gravity loads. For tall buildings on the West Coast of the United States, wall thicknesses typically range from 24 to 42 in. (610 to 1070 mm), and column cross-sectional dimensions typically range from 24 to 48 in. (610 to 1220 mm). Typical unbonded post-tensioned flat-plate floors have thicknesses of approximately 8 in. (203 mm) with spans of approximately 25 to 35 ft (7.6 to 10.7 m), although shorter spans sometimes occur to accommodate architectural requirements.

The two options for construction are either to cast the wall ahead of the slab-column framing and then cast the slab-column framing with connections to the previously cast wall, or to cast each level and its components sequentially along the height of the building. The first option creates a vertical cold joint between the flat plate and the core wall. The cold joint needs to be capable of resisting out-of-plane

ACI Structural Journal, V. 121, No. 2, March 2024.
MS No. S-2023-062.R1, doi: 10.14359/51740250, received September 20, 2023, and reviewed under Institute publication policies.

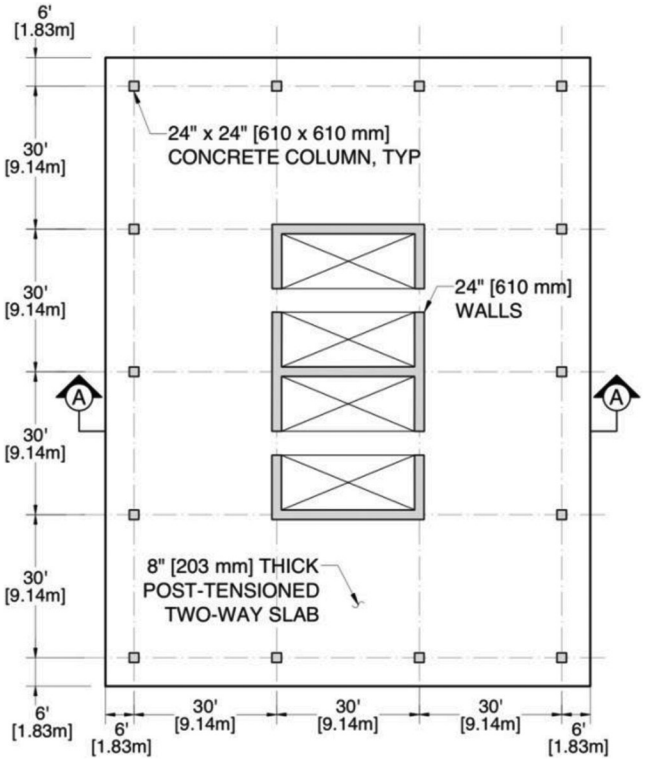

Fig. 1—Plan view of mid-level floor of archetypal tall core-wall building with flat-plate gravity framing.

shear and moment due to gravity and other loads as well as in-plane diaphragm forces, all while sustaining rotations as the building sways under earthquake shaking. A common approach is to anchor the slab post-tensioning just short of the wall and lap-splice it with mild reinforcement that connects across the vertical joint at the wall interface using form-saver mechanical splices. Questions about the performance capability of this connection detail led to the development of a laboratory testing program.

LABORATORY TESTS

Laboratory tests were conducted to study the behavior of the slab-wall-column framing described in the previous section (Klemencic et al. 2006). The present study focuses on Specimen 2 of that test program. The test specimen dimensions are shown in Fig. 2. The 10 ft (3.05 m) width of the specimen represents approximately one-third of a typical span in the transverse direction. The slab had six ASTM A416 Grade 270, 1/2 in. (13 mm) diameter unbonded post-tensioning tendons spaced at 18 in. (457 mm) on center, draped in the longitudinal direction to be 6.5 in. (165 mm) above the bottom of the slab at the column and 1 in. (25 mm) above the bottom of the slab at midspan, with anchors placed one slab thickness (8 in. [203 mm]) from the face of the wall. Figure 3 identifies additional details at the slab-wall connection. The slab-column connection was reinforced with 10 No. 5 (No. 16) top bars centered on the column in each direction and three No. 5 (No. 16) bottom bars through the column cage. All nonprestressed reinforcement was ASTM A615 Grade 60 (Grade 420). The slab-column connection had three stud rails extending from each face, each with nine 1/2 in. (13 mm) diameter studs at 3-3/4 in.

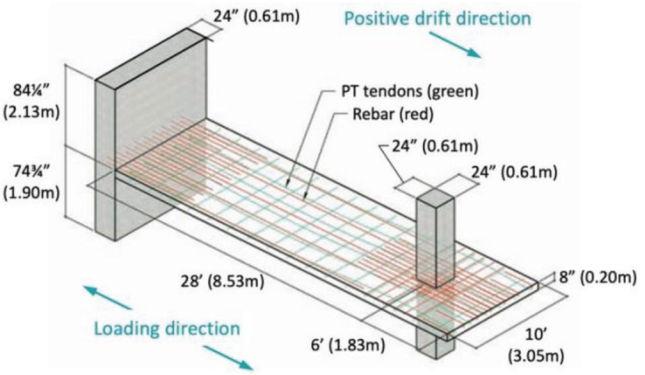

Fig. 2—Isometric view of test specimen (adapted from Klemencic et al. [2006]). (Full-color PDF can be accessed at www.concrete.org.)

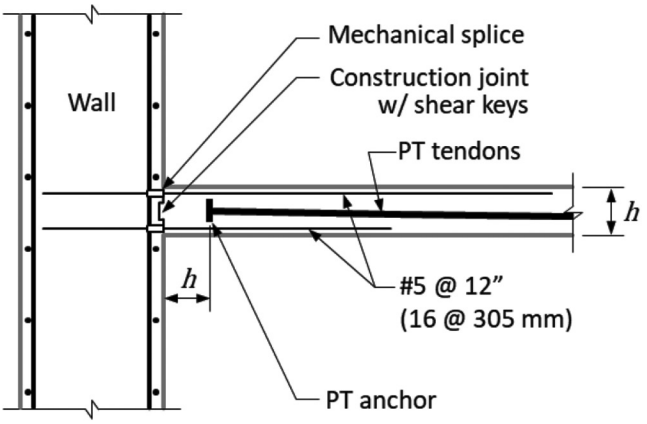

Fig. 3—Test specimen detailing at slab-wall connection for Specimen 2.

(95 mm) spacing made from low-carbon steel C1015 in accordance with ASTM A108 (f_y = 50 ksi [345 MPa]). The mean concrete compressive strength of the slab concrete was 6.1 ksi (42 MPa).

In the test setup, lead weights were distributed over the plan area of the slab to simulate expected superimposed gravity loads of approximately 30.5 lb/ft^2 (1.46 kPa). The wall and column were pinned at the base, and reversed cyclic lateral forces were applied simultaneously at the top of the wall and column in the loading direction, as shown in Fig. 2. The lateral forces resulted in reversed cyclic lateral displacements with progressively increasing amplitudes corresponding to drift ratios. Positive drift ratio was defined as the direction from the wall toward the column. In a real building, loading in the negative direction would subject the wall segment (representing the wall flange) to flexural tension, resulting in wall flange uplift in upper stories that would increase the rotational demands on the slab. To approximate this effect, the testing protocol doubled the imposed displacements for loading in the negative direction (Klemencic et al. 2006).

Figure 4 presents the measured relationship between total lateral force and lateral drift ratio. (The building equivalent drift ratio is defined as the test specimen drift ratio for positive drifts and half those values for negative drifts to approximate the uplift effect described in the previous paragraph.)

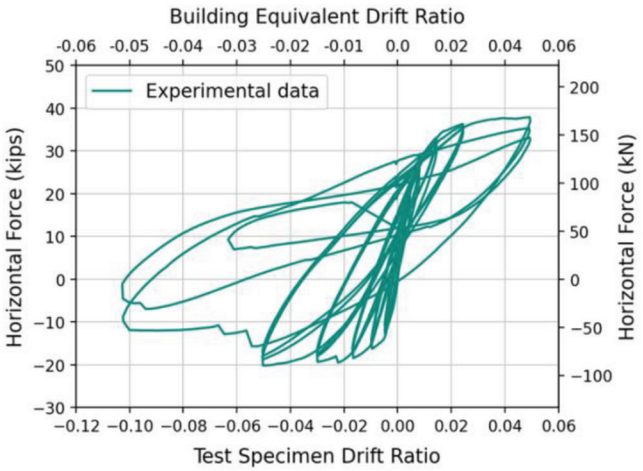

Fig. 4—Measured relationship between total horizontal force and drift ratio.

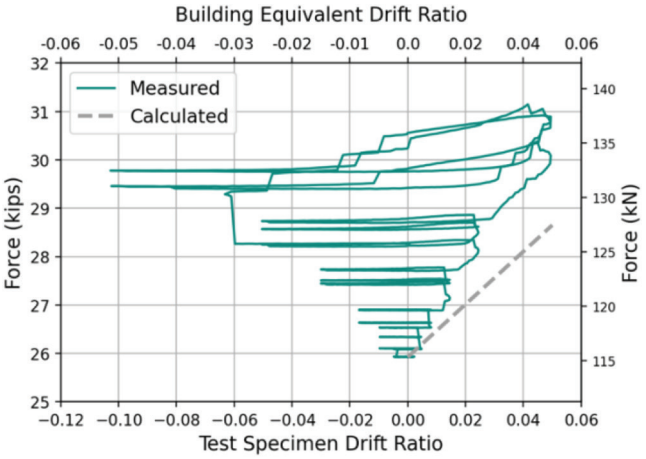

Fig. 5—Measured and calculated strand prestress force versus drift ratio.

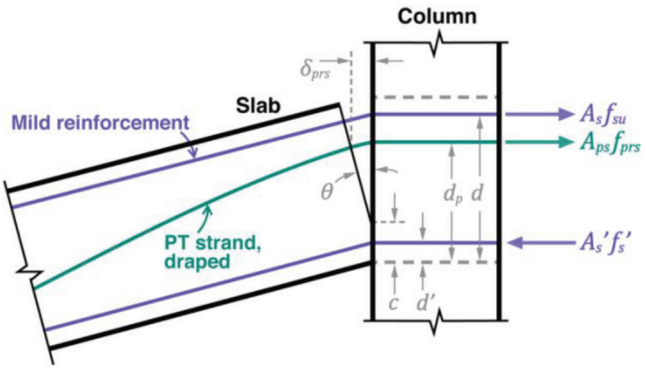

Fig. 6—Rotation of slab-column joint elongates prestressing strand.

The relationship shows nearly linear behavior for small drift ratios with progressively softer, nonlinear behavior as drift amplitudes increased. Strength degradation resulting from the fracture of slab top dowel bars is apparent for building equivalent drift ratios beyond –0.025.

The calculation of slab moment strength requires an estimate of the post-tensioning force in the slab. Figure 5 shows the measured force in a single strand as a function of the test specimen drift ratio. This study is mainly interested in positive drift ratios, as these correspond to hogging rotation in the slab (that is, tension near the top surface) near the slab-column connection. The strand force increases with both increasing lateral drift and repeated cycles at the same drift level.

The increase in post-tensioning force with increasing drift can be explained in terms of the idealized connection deformations shown in Fig. 6, which is adopted from ACI 550.3-13 (Joint ACI-ASCE Committee 550 2013). The interface of the slab and column is assumed to develop a single crack that rotates about the neutral axis. The opening of the crack at the level of the strand is $\delta_{prs} = \theta(d_p - c)$, where θ is the crack opening angle, d_p is the depth from the extreme compression fiber to the centroid of the strand, and c is the flexural compression depth at the probable moment strength. As a simplification, the opening angle θ is approximated as being equal to the drift ratio. If the crack opening produces strand elongation that is spread uniformly along the unbonded strand length L_{ups}, then the change in strain is $\Delta\varepsilon_{prs} = \delta_{prs}/L_{ups}$. Note that a significant change in stress would only occur under positive drift (hogging rotation at the column) because of the 6.5 in. (165 mm) elevation of the strand above the bottom of the slab at the column. A crack opening at the slab-wall connection does not produce strand elongation because the strand stops one slab thickness from the face of the wall. From this model, the change in strand force is $\Delta F_{ps} = A_{ps}E_{ps}\Delta\varepsilon_{ps}$, where the area of a single tendon A_{ps} = 0.153 in.^{2} (98.7 mm^2) and the modulus of elasticity E_{ps} = 27,000 ksi (197,000 MPa). Combining terms, the change in strand force ΔF_{ps} in terms of drift ratio (δ_x/h_{sx}) is

$$\Delta F_{ps} = A_{ps}E_{ps}\frac{d_p - c}{L_{ups}}\left(\frac{\delta_x}{h_{sx}}\right) \quad (1)$$

Figure 5 shows the calculated variation of strand tensile force with increasing drift ratio. The slope of the calculated relationship is close to the slope measured during loading cycles of increasing lateral drift. The calculated relationship falls short of the measured relationship overall, however, because the analytical model does not include the progressive increase in tendon force for repeated load cycles at constant amplitude.

EQUIVALENT FRAME MODELING

Modeling a slab-wall-column framing system using plate-bending elements is usually impractical for nonlinear response-history analysis of a tall building. A more common approach is to subdivide the flat plate into a series of equivalent frames spanning between the wall(s) and columns. Each equivalent frame consists of a slab-beam strip centered on a column representing the mechanical properties of the slab bounded by panel centerlines between columns (Fig. 7). Slab-column connections and slab-wall connections may have different mechanical properties because of their different support conditions. To represent this behavior, the approach adopted (Hwang and Moehle 2000) divides the slab-beam at the midpoint of the span, with different beam effective widths in the two beam halves (Fig. 7).

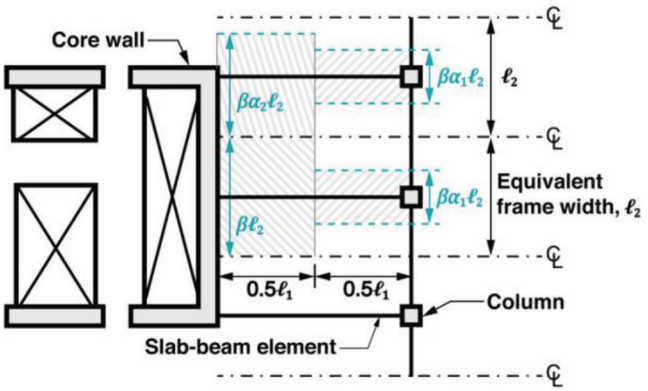

Fig. 7—Framing system is modeled using series of equivalent beam-column-wall frames.

In a complete building model, nonlinear behavior may occur in the slab, columns, and walls. A nonlinear response can be represented using a variety of nonlinear modeling approaches (for example, PEER TBI [2017]). To model the laboratory test specimen (Fig. 2), the model shown in Fig. 8 is adopted. The slab-beam model consists of three linear-elastic beam elements: one for the half span nearer the column, one for the half span nearer the wall, and another for the slab cantilever. A bilinear hysteretic moment-rotation hinge was placed at each end of the beam to represent the nonlinear slab-wall or slab-column response, which corresponds to a lateral side-sway mechanism that was confirmed by structural analysis. (Hinges distributed along the span should also be considered in cases where hinging could occur along the slab span.) The column and wall were significantly stronger than the slab connections and, consequently, were modeled using linear-elastic line elements.

Slab effective lateral stiffness

When a slab-column connection is subjected to lateral loading, the slab experiences moments and rotations that are largest near the column and decrease with increasing transverse distance from the column. Vanderbilt and Corley (1983) describe an equivalent or effective beam-width model in which the slab is replaced by a prismatic beam of width $b_e = \alpha\ell_2$ having equivalent rotational stiffness, where the coefficient α accounts for the nonuniform rotation of the slab across its width, and ℓ_2 is the width of the slab panel perpendicular to the direction that slab moments are being determined (Fig. 7). Flexural stiffness is calculated from the gross section of the slab considering the slab-beam effective width and total thickness h. Vanderbilt and Corley (1983) proposed an additional reduction factor β to account for the effect of slab cracking on effective stiffness.

Hwang and Moehle (2000) proposed that the coefficient b_e for interior slab-column connections be determined as

$$b_e = 2c_1 + \ell_1/3 \tag{2}$$

where c_1 is the dimension of the rectangular or equivalent rectangular column measured in the direction of the span ℓ_1, where ℓ_1 is the span length in the direction that moments are being determined, measured center-to-center of supports.

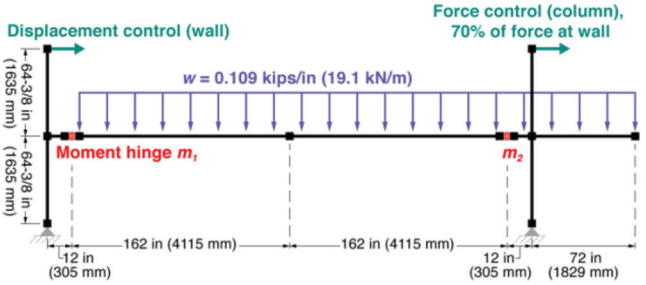

Fig. 8—Analytical model of specimen from laboratory test.

The equation was derived from the results of elastic-plate theory and finite element analyses for slab panels having $2/3 \le \ell_2/\ell_1 \le 3/2$. It is intended to be used in an analytical model that represents the slab-column joints as rigid. For a slab-wall connection in which the slab frames into the wall flange along its entire width, $b_e = \ell_2$ should be used. Based on a study summarized in Appendix A, for a slab-wall connection in which the slab frames into the wall flange along only a portion of its width, the value of b_e can be taken equal to the contact width plus 0.7 times the width of the equivalent frame extending beyond the flange.

For nonprestressed slabs, Hwang and Moehle (2000) proposed

$$\beta = \frac{4c_1}{\ell_1} \ge \frac{1}{3} \tag{3}$$

The lower limit of β = 1/3 is consistent with the proposal by Vanderbilt and Corley (1983). For post-tensioned slabs, Kang and Wallace (2005) proposed a lower limit of β = 1/2, considering reduced cracking due to the compression effects of prestressing. This approach to stiffness modeling using an effective beam width is recognized in ASCE/SEI 41-17 (2017).

In a building model where column and wall yielding might occur, the adopted analytical models should adequately represent the effects of axial-flexural interaction. For walls, it is also important to model flange uplift associated with axial elongation and neutral axis migration. For modeling this test specimen, however, inelastic response and uplift are not expected, so linear-elastic line elements are adopted for columns and walls.

The effective width represented by Eq. (2) is not directly applicable to the slab-column connection of the laboratory test structure because the transverse dimension of the test slab (Fig. 2) is only approximately one-third of the transverse span in a typical building (Fig. 1), and the slab aspect ratio falls outside the range for which Eq. (2) was derived. If this limitation is ignored, then the calculated effective width at the slab-column connection is equal to $b_e = 2 \cdot 24$ in. + 348 in./3 = 164 in. (2 · 0.61 m + 8.84 m/3 = 4.27 m), which exceeds the provided width of 120 in. (3.05 m). Here, b_e = 120 in. (3.05 m) is taken at both the column and wall connections, which is the correct value at the slab-wall connection but slightly overestimates the effective width at the slab-column connection. To account for slab cracking, the additional stiffness reduction factor β = 1/2 is applied.

Table 1—Summary of strength limits at slab-column connection

Strength limit		Expected strength at critical section	Moment strength at column face, kip·in. (kN·m)
(a) One-way shear strength of full slab		V_n = 162 kip (719 kN)*	23,000 (2600)
(b) Flexural strength of full slab	Hogging	M_{pr} = 3150 kip·in. (360 kN·m)	3150 (360)
	Sagging	M_{pr} = 1260 kip·in. (143 kN·m)	1260 (143)
(c) Flexural strength of effective transfer width	Hogging	M_{pr} = 1810 kip·in. (205 kN·m)	3020 (342)
	Sagging	M_{pr} = 764 kip·in. (86.3 kN·m)	1270 (144)
(d) Two-way shear transferred across connection		M_{sc} = 8490 kip·in. (960 kN·m)†	8030 (908)

*Located at $h/2$ from the face of the column.

†Located at the center of the critical section.

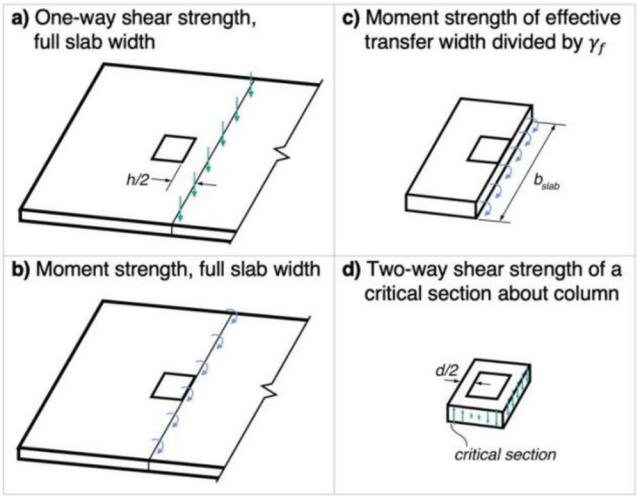

Fig. 9—Four limits on strength at slab-column connection.

Slab-wall and slab-column connection strengths

In the general case, connection strength can be limited by either the strength of the slab or the strength of the supporting column or wall. In the test structure (Fig. 2), as in most tall buildings, connection strength is limited by the slab.

The slab-wall connection strength is taken as the probable moment strength M_{pr} following the method in ACI 318. Zero axial force in the slab is assumed because the prestressing stops short of the wall (Fig. 3) and the externally applied forces in the test setup produce negligible slab axial force. (In a real building, however, there may be some in-plane inertial forces and precompression from the post-tensioned slab extending around the core wall.) Considering top and bottom Grade 60 No. 5 at 12 in. (Grade 420 No. 16 at 305 mm), the probable moment strength based on a maximum bar stress capacity of $1.25f_y$ is calculated as 1640 kip·in. (185 kN·m). One-way shear strength at the connection with the wall does not limit connection moment transfer strength.

At a slab-column connection, strength can be limited by four different strength quantities (Fig. 9): 1) one-way shear strength of the full transverse width of the slab; 2) moment strength of the full transverse width of the slab; 3) moment transfer strength as limited by slab moment capacity near the column; and 4) two-way shear strength of a critical section about the column.

The one-way nominal shear strength of the full transverse width of the slab is the sum of shear strength contributions from concrete and shear reinforcement, $V_n = V_c + V_s$, taken at the critical section for prestressed slabs located at a distance $h/2$ from the face of the column. V_c is calculated following ACI 318 for concrete shear strength in prestressed flexural members, where V_c is the lesser of the flexure-shear strength and web-shear strength. The shear capacity provided by shear reinforcement in the form of three stud rails is $V_s = 3A_v f_{yt} d/s$, where A_v is the area of a single stud, f_{yt} is the stud yield strength, d is the effective depth of the slab (taken as at least $0.8h$ for prestressed two-way slabs), and s is the spacing of the studs measured perpendicular to the assumed one-way shear failure line. The moment at the face of the column corresponding to the development of V_n at $h/2$ from the face was estimated using a linear-elastic analytical model with geometry similar to the one shown in Fig. 8. The resulting moment greatly exceeded moments corresponding to other failure modes (Table 1), such that the details of the calculation were not critical.

The moment strength of the full transverse width of the slab is adapted from the ACI 318 method for the probable moment strength M_{pr}. The strain of the concrete section and bonded reinforcement is assumed to vary linearly through depth, with a peak compressive strain equal to 0.003. Stress in the bonded reinforcement is proportional to strain, up to a limiting stress of $1.25f_y$. Force in the unbonded prestressing strands is assumed to vary with lateral drift ratio, as described previously in relation to Fig. 6 and Eq. (1). The depth to the neutral axis c is obtained from iteration, assuming the axial force in the post-tensioned section is equal to the number of post-tensioning tendons multiplied by the calculated final prestress force per tendon, F_{ps}. Given the specified effective prestress force F_{pe} = 26.8 kip/strand (119 kN) before testing and the drift ratio at MCE_R demand levels is assumed equal to 1.5 times the design limit of 0.02, the calculated final prestress force F_{ps} for hogging rotation is

$$\Delta F_{ps} = A_{ps}E_{ps}\frac{d_p - c}{L_{ups}}\left(\frac{\Delta_x}{h_{sx}}\right) =$$

$$(0.153\ \text{in.}^2)(27{,}000\ \text{ksi})\left(\frac{6.5\ \text{in.} - 1.22\ \text{in.}}{400\ \text{in.}}\right)(0.03) = 1.64\ \text{kip}$$

$$\left[(9.871 \times 10^{-5}\ \text{m}^2)(186{,}200\ \text{MPa})\left(\frac{0.1651\ \text{m} - 0.0310\ \text{m}}{10.16\ \text{m}}\right)\right.$$

$$\left. = 7.28\ \text{kN}\right]$$

$$F_{ps} = F_{pe} + \Delta F_{ps} = 28.4\ \text{kip}\ (126\ \text{kN})$$

The resulting probable moment strength is M_{pr} = 3150 kip·in. (360 kN·m) for the top of the slab in tension and M_{pr} = 1260 kip·in. (143 kN·m) for the bottom of the slab in tension.

The slab-column connection moment transfer strength should also be checked using the two-way shear strength design model of ACI 318 and ACI 352.1R-11 (Joint ACI-ASCE Committee 352 2012). This requires checking both a bending moment strength limit and a two-way shear stress limit. According to the model, a fraction γ_f of the total connection transfer moment M_{sc} is resisted by slab flexure across a width b_{slab} centered on the column and extending 1.5 slab thicknesses on both sides of the column. γ_f = 0.6 for columns with a square cross section (ACI 318). Following procedures for calculating probable moment strength outlined previously, M_{pr} = 1810 kip·in. (205 kN·m) for a width b_{slab} when the top of the slab is in tension. The moment transfer strength limited by slab flexure when loading in the positive direction is $M_{sc} = M_{pr}/\gamma_f$ = 3020 kip·in. (342 kN·m). Using the same procedure for the bottom of the slab in tension, a moment transfer strength limited by slab flexure is calculated as M_{sc} = 1270 kip·in. (144 kN·m).

The moment transfer strength can also be limited by the two-way shear strength of a critical section about the column. According to the model in ACI 318, the combination of direct shear V_u and moment transfer M_{sc} produces shear stress v_u that varies linearly along a critical section located $d/2$ from the column face, as defined by Eq. (4)

$$v_u = \frac{V_u}{b_o d} \pm \frac{\gamma_v M_{sc} c'}{J_c} \quad (4)$$

where b_o is the perimeter of the critical section for two-way shear, $\gamma_v = 1 - \gamma_f$; c' is the distance from the centroid of the critical section to the location of the shear stresses v_u; and J_c is the equivalent of the polar moment of inertia for the slab critical section. Details for the calculation of v_u in Eq. (4) are provided in ACI 318 and standard texts (for example, Wight [2016]). For design, the ultimate shear stress v_u is compared with a design shear-stress capacity ϕv_n, and from Eq. (4), M_{sc} can be solved as limited by nominal two-way slab shear capacity stress. For test specimens and checks at MCE_R loading, ϕ = 1.0. The resulting moment capacity is M_{sc} = 8490 kip·in. (960 kN·m). M_{sc} is defined at the center of the critical section and is transferred to the column face using the linear-elastic model, as described previously for one-way shear, resulting in a moment capacity of 8030 kip·in. (908 kN·m) at the face of the column.

Comparison of measured and calculated force-displacement relationships

The analytical model of Fig. 8 was implemented in the finite element software OpenSees (McKenna et al. 2010). The nonlinear moment hinges representing the slab-wall (m_1) and slab-column (m_2) connections were modeled with zero-length plastic hinges using a uniaxial bilinear hysteretic material ("Hysteretic"), with strengths limited by the smallest values calculated in the preceding section considering various possible limiting strengths. The deformation

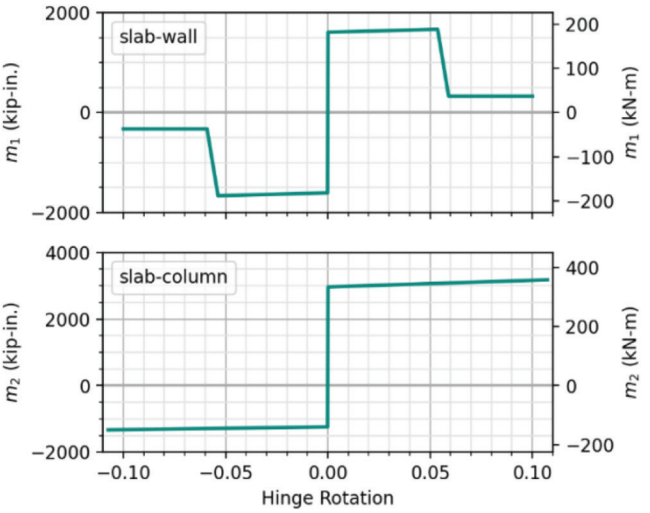

Fig. 10—Moment-rotation hinge properties at slab-wall (m_1) and slab-column (m_2) connections.

capacities of the moment hinges were calibrated based on the observations from the laboratory experiment, with the limiting envelope relationships shown in Fig. 10. Both hinges are bilinear with infinite initial stiffness and reach their calculated moment strength at a rotation of 0.032, corresponding to a drift ratio of 0.03 at MCE_R demand levels. A nominal amount of strain hardening (2%) was incorporated to reflect material strain hardening at both connections. The slab-wall hinge has a strength drop at a rotation of ±0.054, corresponding to a drift ratio of 0.05, which is when, during the experiment, several top bars at the slab-wall connection fractured. The residual strength of the slab-wall hinge is approximated as one-fifth of the calculated hinge strength. The slab-column connection performed well until the end of the test, so a rotation capacity of ±0.10 was somewhat arbitrarily assigned for the connection. Data reported in ACI 352.1R-11 suggest a median rotation capacity of approximately 0.05 for nonprestressed slabs with shear reinforcement, and a larger capacity would generally be expected for post-tensioned slabs. The hysteretic response of the model was calibrated using the hysteretic material parameters for pinching, damage, and unloading stiffness to achieve strength degradation similar to the experimental data. The OpenSees result was checked using an elastic-perfectly plastic limit analysis with good results.

Figure 11 compares the measured and calculated force-displacement relationships. The figure inset shows the first load cycles up to a drift ratio of 0.005, showing that the initial stiffness of the analytical model is in agreement with that of the test results. The upper limit of force measured during the experiment closely matches the upper limit of the force in the OpenSees analytical model for loading in the positive direction. In the negative direction of loading, the model overestimates strength. A plausible reason for the overestimation is that the effective slab width for moment transfer, b_{slab}, is not applicable when the bottom of the slab is in tension. However, even when reducing the effective slab width to the width of the column, 24 in. (610 mm), the model still overestimates strength in the negative direction by approximately 20%. It is possible that the hogging

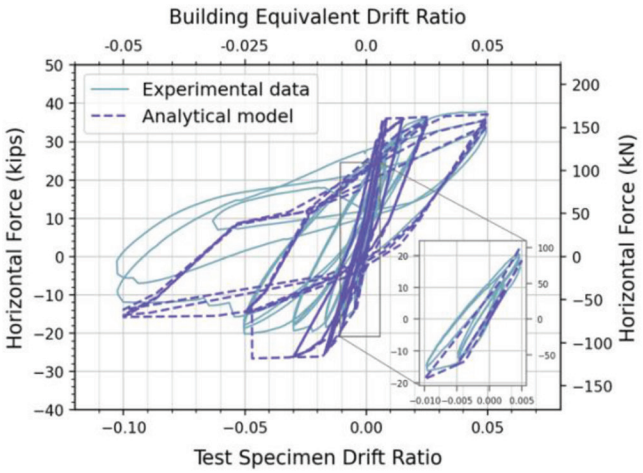

Fig. 11—Comparison of calculated plastic capacity from analytical model to experimental results from test specimen.

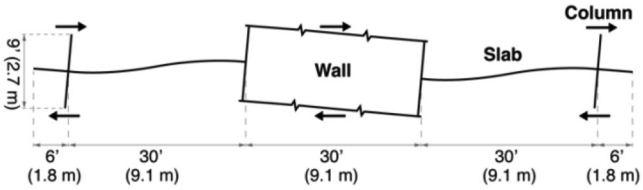

Fig. 12—Elevation view of example structure through section A-A (Fig. 1) under rotation from lateral earthquake forces.

moment from the gravity load applied to the slab was not overcome by the lateral load in the negative direction at the drift ratios from the laboratory test, leading to the slab not fully developing its strength with the bottom of the slab-column joint in tension.

EXAMPLE CALCULATION: OUTRIGGER EFFECT ON COLUMN AXIAL FORCES

This section presents an example calculation to illustrate the effect of slab-column outrigger framing on column axial forces for an archetypical tall core-wall building with 40 stories. The building is assumed to be located in San Francisco, CA, assigned to Risk Category II, at a site with Site Class C, Seismic Design Category D, and S_{DS} = 1.2g (ASCE/SEI 7). The building has a regular floor plan, as shown in Fig. 1, and a typical story height of 9 ft (2.7 m). Table 2 lists the design dead and live loads.

Forces in this example are calculated for a typical edge column in a single story using the ASCE/SEI 7 load combinations, assuming the slab-column frame is not a part of the lateral-force-resisting system and considering lateral loading in one horizontal direction only. The axial force is calculated for a single story at the column shown on the right in Fig. 12. The forces would sum over the height of the building for the total column axial force, although it is plausible that not all the axial forces are at their peak value at the same time. The dead and live loads on the column are found using the tributary area method. The live loads are reduced by a factor of 0.4. By ASCE/SEI 7, columns should be designed for four load combinations: 1.4D, 1.2D + 1.6L, 1.2D + 0.5L + E, and 0.9D – E, where E does not include the horizontal earthquake force E_h because the slab-column framing is assumed not to contribute to the lateral resistance of the building. Horizontal earthquake forces cause the "outrigger effect" on the slab-column gravity framing and increase the axial forces on the columns. This example compares the effect of including the horizontal earthquake load on the column axial force.

Table 2—Assumed dead and live loads

	Load source	Distributed load
Dead	Slab self-weight	100 lb/ft^2 (4.79 kPa)
	Additional per floor	25 lb/ft^2 (1.20 kPa)
	Cladding (perimeter)	15 lb/ft^2 (0.72 kPa)
	Column self-weight	600 lb/ft (8.76 kN/m)
Live	Offices	50 lb/ft^2 (2.39 kPa)

Table 3—Resulting column axial force for each load combination

Case No.	Load combination	Column axial force, kip (kN)	
		Without E_h	With E_h
1	1.4D	123 (549)	
2	1.2D + 1.6L	126 (560)	
3	1.2D + 0.5L + E_v + E_h	133 (593)	153 (681)
4	0.9D – E_v – E_h	58.2 (259)	37.3 (166)

The horizontal earthquake force E_h is taken as the lateral capacity of the slab-wall-column subsystem. The value of the axial force on the column for each of the four load cases is calculated with and without the inclusion of the horizontal earthquake force E_h.

The moment strength of the slab-wall connection is calculated according to the method for M_{pr} from ACI 318 for the slab section at the wall, using Grade 60 No. 5 at 12 in. (No. 16 at 305 mm) top and bottom, similar to the test specimen configuration. The section analysis of the full slab cross section with a width of 30 ft (9.14 m) results in a probable moment strength of 4920 kip·in. (556 kN·m) at the slab-wall connection. The slab-column connection in this example is identical to that of the test specimen, except the transverse dimension of the slab is 30 ft (9.14 m). Of the four checks for limiting moment strength, the moment strength, when limited by one-way shear, greatly exceeds moments corresponding to other failure modes. The one-way moment strength of the slab is M_{pr} = 3450 kip·in. (390 kN·m) at the column face. The moment transfer strength in flexure is the same as that of the test specimen when using an effective transfer width of $b_{slab} = c_2 + 3h$, while the moment transfer strength in two-way shear is M_{sc} = 6690 kip·in. (756 kN·m), which translates to 6810 kip·in. (770 kN·m) at the column face. The limiting moment strength at the slab-column connection is controlled by the moment transfer strength in flexure, M_{sc} = 3040 kip·in. (344 kN·m).

The resulting column axial forces calculated for the right-hand column are shown in Table 3. The column axial force increases by 15% for load combination 3 (1.2D + 0.5L + E) when including the effect of the horizontal earthquake load. The substantial increase in axial force when accounting for the outrigger action of gravity framing under earthquake

loading indicates that earthquake loads may be significant enough to control the axial design of gravity columns in tall buildings with flat-plate gravity framing. This example demonstrates that for a structure with the given dimensions, which are typical among tall core-wall buildings, neglecting the behavior of the slab outriggers may result in underdesigned gravity columns. The outrigger effect on column axial force would tend to increase for columns located closer to the core wall than is assumed in this example.

SUMMARY AND CONCLUSIONS

Many tall core-wall buildings use unbonded post-tensioned flat-plate gravity framing with perimeter columns. This framing participates in resisting lateral forces as a building sways under earthquake shaking and produces outrigger action that affects column axial forces. The outrigger effect can also modify the overall building dynamic properties and dynamic response, as well as modify the wall shears due to the frame-wall interaction between the wall and the outrigger slab-column frame. However, these additional effects are beyond the scope of this paper, which focuses instead on the outrigger modeling problem. An analytical model using outrigger slab-beams was developed to demonstrate an effective method for modeling the stiffness, strength, and nonlinear force-deformation relationship of a slab-wall-column frame. The outrigger beams had stiffness based on the effective beam-width model and strengths based on expected strengths calculated in accordance with ACI 318. The analytical model was calibrated to previous laboratory testing by Klemencic et al. (2006). Results of the analytical model were used to study the likely effects of outrigger action on the design axial forces for columns in an archetypal tall building.

The output load-deformation response from the analytical simulation showed that the effective beam-width model estimated the lateral stiffness of a slab-wall-column framing very well compared with test data. As part of the calculation for probable moment strength in a post-tensioned slab, a linear relationship was defined for the change in force due to the elongation of the post-tensioning tendons with an increasing drift ratio. The strength estimates for the slab-wall and slab-column connections gave a good estimate of peak lateral force in the positive direction (slab top in tension at the slab-column connection) and an overestimate in the negative direction compared with test data.

For the given example story of a tall building, accounting for the outrigger effect by including horizontal earthquake loads in design load combinations for the gravity framing system resulted in a 15% increase in column axial force in a single story. The effect of this discrepancy may also be amplified over many stories in a tall building. It is recommended to include the outrigger effect in typical tall buildings to obtain a better estimate of column design axial force.

AUTHOR BIOS

Connie I. Chen *received her BS, MS, and PhD from the University of California, Berkeley, Berkeley, CA. She received the 2019 National Science Foundation (NSF) Graduate Research Fellowship and the 2022-2023 Earthquake Engineering Research Institute (EERI)/Federal Emergency Management Agency (FEMA) National Earthquake Hazards Reduction Program (NEHRP) Graduate Fellowship. Her research interests include tall buildings, reinforced concrete structures, and earthquake engineering.*

ACI Honorary Member **Jack P. Moehle** *is a Professor at the Graduate School in Civil and Environmental Engineering at the University of California, Berkeley. He is past Chair of ACI Committee 318, Structural Concrete Building Code. His research interests include the design and analysis of structural systems, with an emphasis on earthquake engineering, reinforced concrete construction, and the development of professional design guidance.*

ACKNOWLEDGMENTS

This material is based upon work supported by the National Science Foundation Graduate Research Fellowship under Grant No. DGE 1752814. Any opinions, findings, and conclusions or recommendations expressed in this material are those of the authors and do not necessarily reflect the views of the National Science Foundation.

NOTATION

A_{ps}	=	area of single post-tensioned tendon
A_v	=	area of single shear stud
b_e	=	effective beam width
b_o	=	perimeter of critical section for two-way shear at slab-column connection
b_{slab}	=	effective slab width for moment transfer in flexure at column
c	=	flexural compression depth at probable moment strength
c'	=	distance from centroid of column critical section to location of eccentric shear stresses
c_1	=	dimension of rectangular column parallel to direction of loading
c_2	=	dimension of rectangular column perpendicular to c_1
d	=	slab effective depth
d_p	=	depth from extreme compression fiber to centroid of post-tensioned reinforcement
E_{ps}	=	modulus of elasticity of prestressing steel
F_{pe}	=	specified effective prestress force
F_{ps}	=	final force in prestressing steel
f_y	=	yield stress of nonprestressed steel
f_{yt}	=	yield stress of shear reinforcing steel
h	=	slab thickness
h_{sx}	=	height at story x
J_c	=	equivalent of polar moment of inertia for slab critical section in two-way shear
L_{ups}	=	length of unbonded post-tensioning steel
ℓ_1	=	length of span parallel to direction of loading
ℓ_2	=	length of span perpendicular to direction of loading
M_{pr}	=	probable moment strength
M_{sc}	=	moment transfer strength about slab-column connection
s	=	spacing of shear studs measured parallel to rail
V_c	=	shear strength contribution from concrete
V_n	=	one-way nominal shear strength
V_s	=	shear strength contribution from shear reinforcement
V_u	=	factored shear demand
v_u	=	shear stress along column critical section in two-way shear
w	=	distributed load
α	=	factor of stiffness reduction due to rotation across transverse width of slab
β	=	factor of stiffness reduction due to concrete cracking
δ_{prs}	=	width of crack opening at height of post-tensioning steel at slab-column connection
δ_x	=	lateral drift at story x
ε_{prs}	=	strain in prestressing steel
γ_f	=	fraction of transfer moment M_{sc} transferred by slab flexure
γ_v	=	fraction of transfer moment M_{sc} transferred by slab shear stress
θ	=	opening angle of crack at slab-column connection

REFERENCES

ACI Committee 318, 2019, "Building Code Requirements for Structural Concrete (ACI 318-19) and Commentary (ACI 318R-19) (Reapproved 2022)," American Concrete Institute, Farmington Hills, MI, 624 pp.

ASCE/SEI 7-16, 2017, "Minimum Design Loads and Associated Criteria for Buildings and Other Structures," American Society of Civil Engineers, Reston, VA, 800 pp.

ASCE/SEI 41-17, 2017, "Seismic Evaluation and Retrofit of Existing Buildings," American Society of Civil Engineers, Reston, VA, 576 pp.

CSI, 2021, "SAP2000 Integrated Software for Structural Analysis and Design, v23.3.0" Computers and Structures, Inc., Walnut Creek, CA.

Hwang, S.-J., and Moehle, J. P., 2000, "Models for Laterally Loaded Slab-Column Frames," *ACI Structural Journal*, V. 97, No. 2, Mar.-Apr., pp. 345-352.

Joint ACI-ASCE Committee 352, 2012, "Guide for Design of Slab-Column Connections in Monolithic Concrete Structures (ACI 352.1R-11)," American Concrete Institute, Farmington Hills, MI, 28 pp.

Joint ACI-ASCE Committee 550, 2013, "Design Specification for Unbonded Post-Tensioned Precast Concrete Special Moment Frames Satisfying ACI 374.1 (ACI 550.3-13) and Commentary (Reapproved 2022)," American Concrete Institute, Farmington Hills, MI, 28 pp.

Kang, T. H.-K., and Wallace, J. W., 2005, "Dynamic Responses of Flat Plate Systems with Shear Reinforcement," *ACI Structural Journal*, V. 102, No. 5, Sept.-Oct., pp. 763-773.

Klemencic, R.; Fry, J. A.; Hurtado, G.; and Moehle, J. P., 2006, "Performance of Post-Tensioned Slab-Core Wall Connections," *PTI Journal*, V. 4, No. 2, Dec., pp. 7-23.

LATBSDC, 2020, "An Alternative Procedure for Seismic Analysis and Design of Tall Buildings Located in the Los Angeles Region," Los Angeles Tall Buildings Structural Design Council, Los Angeles, CA, 92 pp.

McKenna, F.; Scott, M. H.; and Fenves, G. L., 2010, "Nonlinear Finite-Element Analysis Software Architecture Using Object Composition," *Journal of Computing in Civil Engineering*, ASCE, V. 24, No. 1, Jan., pp. 95-107.

PEER TBI, 2017, "Guidelines for Performance-Based Seismic Design of Tall Buildings," PEER Report No. 2017/06, Version 2.03, Tall Buildings Initiative, Pacific Earthquake Engineering Research Center, University of California, Berkeley, Berkeley, CA, 143 pp.

Vanderbilt, M. D., and Corley, W. G., 1983, "Frame Analysis of Concrete Buildings," *Concrete International*, V. 5, No. 12, Dec., pp. 33-43.

Wight, J. K., 2016, *Reinforced Concrete: Mechanics and Design*, seventh edition, Pearson Education, Hoboken, NJ, 1168 pp.

APPENDIX A: EFFECTIVE BEAM WIDTH FOR SLAB WITH PARTIAL CONNECTIVITY TO WALL

A study was done to calculate the moment-rotation stiffness of a slab-wall connection in which the slab connects directly to a flanged wall along half of the slab equivalent frame width. An alternative approach would be required for a slab framing into the edge of a blade wall. Figure A1 shows the overall geometry of the assumed floor system with the equivalent frame under consideration shown shaded.

A linear-elastic model of the equivalent frame was implemented using the software SAP2000 (CSI 2021). The slab was modeled using thin shell elements with infinite in-plane rigidity. Slab free edges were unrestrained, while the edges parallel to the equivalent frame (dashed lines in Fig. A1) were restrained to have zero rotation about the dashed lines. The wall and columns, including the regions common to the slab, wall, and columns, were modeled as rigid. Shear deformations were neglected, and a Poisson's ratio of 0.2 was assumed.

Two different imposed deformation patterns were considered. In the first, the core wall was assumed to rotate about gridline D in Fig. A1. This deformation pattern is considered to be representative of deformations occurring in the lower stories of a tall core-wall building and is referred to as the lower-story condition. In the second pattern, the core wall was assumed to rotate about gridline E. This deformation pattern is considered to be more representative of deformations occurring in the upper stories of a tall core-wall building, where accumulation of flexural tension strain in the tension flange has resulted in wall uplift and is referred to as the upper-story condition. In both cases, the columns were assumed to rotate about their centroid at the base of the column. A unit rotation was imposed on the wall and columns in both deformation patterns.

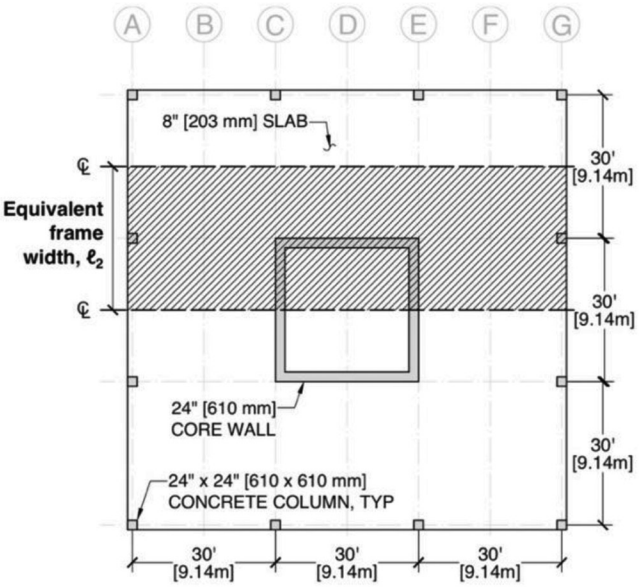

Fig. A1—Floor plan used for finite element model.

Table A1—Effective beam width coefficients

		Span AC	Span EG
Lower-story boundary condition	b/ℓ_2 at column*	0.40	0.40
	b/ℓ_2 at wall	0.88	0.88
Upper-story boundary condition	b/ℓ_2 at column*	0.39	0.42
	b/ℓ_2 at wall	0.90	0.83

*Compare with Hwang and Moehle (2000); b_e/ℓ_2 = 168 in./360 in. = 0.47.

The effective beam width coefficient was found by first determining the stiffness of the model with the full slab modeled using shell elements. The slabs in each equivalent frame are divided at the midpoint of the span and replaced with beams of effective widths, calibrated such that the beam end moment matches the total moment in the slab across the equivalent frame width at the wall and the column. Table A1 lists the resulting effective beam widths.

Note that the calibrated effective beam widths on the column side are smaller than the values calculated from Hwang and Moehle (2000). The difference may relate to the different geometries of the framing spans, different modeling assumptions, and approximations in deriving the factors in Hwang and Moehle (2000).

The effective beam width coefficients ranged from 0.83 to 0.90 and were not strongly affected by the two different rotation axes considered. The effective beam width in this study comprised half the width of the equivalent frame that was rigidly connected to the wall, plus an additional effective width for the other half of the equivalent frame extending beyond the wall. In the interest of simplicity and applicability to a wider range of geometries, it is recommended to use an effective width equal to the width of contact between the slab and wall plus 0.7 times the width of the equivalent frame extending beyond the wall.

ARE YOU A RESEARCHER?

SIGN UP FOR ORCID TODAY!

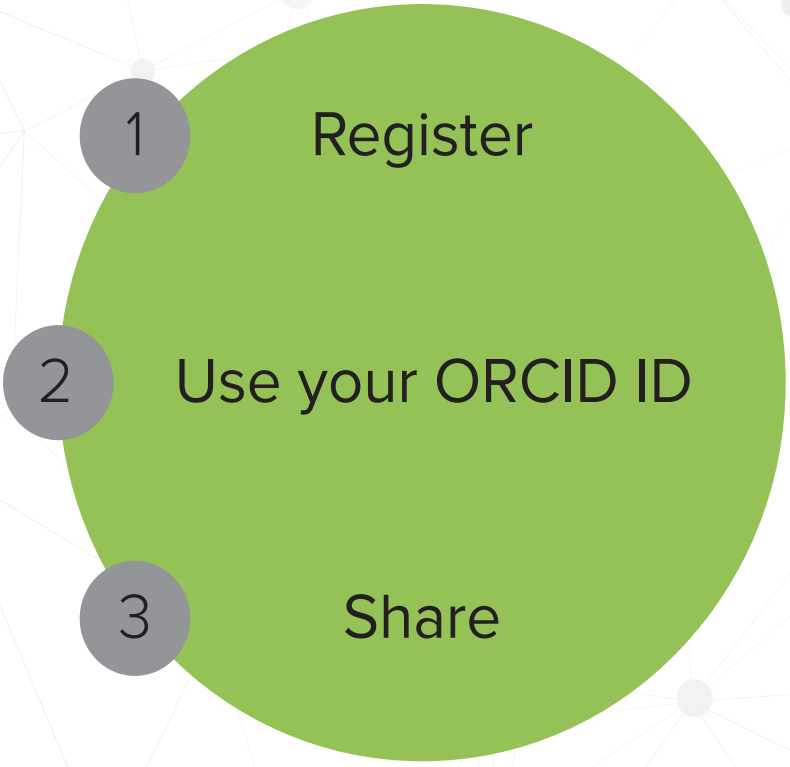

ORCID provides a digital identifier that distinguishes you from every other researcher and, through integration in key research workflows such as manuscript and grant submission, supports automated linkages between you and your professional activities, ensuring that your work is recognized.

ORCID services are FREE and it's as easy as **1-2-3**.

WWW.ORCID.ORG